

Hardening effect of multi-energy W^{2+}-ion irradiation on tungsten-potassium alloy

Yang-Yi-Peng Song(宋阳一鹏), Wen-Bin Qiu(邱文彬), Long-Qing Chen(陈龙庆), Xiao-Liang Yang(杨晓亮), Hao Deng(邓浩), Chang-Song Liu(刘长松), Kun Zhang(张坤), Jun Tang(唐军)

Citation: Chin. Phys. B . 2020, 29(10): 105202 . **doi:** 10.1088/1674-1056/ab9c09
Journal homepage: http://cpb.iphy.ac.cn; http://iopscience.iop.org/cpb

What follows is a list of articles you may be interested in

Radiative divertor behavior and physics in Ar seeded plasma on EAST

Jingbo Chen(陈竞博), Yanmin Duan(段艳敏), Zhongshi Yang(杨钟时), Liang Wang(王亮), Kai Wu(吴凯), Kedong Li(李克栋), Fang Ding(丁芳), Hongmin Mao(毛红敏), Jichan Xu(许吉禅), Wei Gao(高伟), Ling Zhang(张凌), Jinhua Wu(吴金华), Guang-Nan Luo(罗广南), EAST Team

Chin. Phys. B . 2017, 26(9): 095205 . **doi:** 10.1088/1674-1056/26/9/095205

Optical waveguide in Nd: $Bi_{12}SiO_{20}$ crystal produced bymulti-energy C ion implantation

Tao Liu(刘涛), Wei-Jin Kong(孔伟金), Ying-Ying Ren(任莹莹), Yan Cheng(成燕)

Chin. Phys. B . 2017, 26(7): 076105 . **doi:** 10.1088/1674-1056/26/7/076105

Structural and mechanical properties of Al-C-N films deposited at room temperature by plasma focus device

Z A Umar, R Ahmad, R S Rawat, M A Baig, J Siddiqui, T Hussain

Chin. Phys. B . 2016, 25(7): 075201 . **doi:** 10.1088/1674-1056/25/7/075201

Mechanical properties of Al/a-C nanocomposite thin films synthesized using a plasma focus device

Z. A. Umar, R. S. Rawat, R. Ahmad, A. K. Kumar, Y. Wang, T. Hussain, Z. Chen, L. Shen, Z. Zhang

Chin. Phys. B . 2014, 23(2): 025204 . **doi:** 10.1088/1674-1056/23/2/025204

X-ray spectra of high temperature tungsten plasma calculated with collisional radiative model

Wang Jun, Zhang Hong, Cheng Xin-Lu

Chin. Phys. B . 2013, 22(8): 085201 . **doi:** 10.1088/1674-1056/22/8/085201

Hardening effect of multi-energy W^{2+}-ion irradiation on tungsten–potassium alloy*

Yang-Yi-Peng Song(宋阳一鹏)[1], Wen-Bin Qiu(邱文彬)[1], Long-Qing Chen(陈龙庆)[1], Xiao-Liang Yang(杨晓亮)[1], Hao Deng(邓浩)[1], Chang-Song Liu(刘长松)[2], Kun Zhang(张坤)[1,†], and Jun Tang(唐军)[1,‡]

[1] *Key Laboratory of Radiation Physics and Technology of Ministry of Education, Institute of Nuclear Science and Technology, Sichuan University, Chengdu* 610064, *China*

[2] *Key Laboratory of Materials Physics, Institute of Solid State Physics, Chinese Academy of Sciences, Hefei* 230031, *China*

(Received 24 February 2020; revised manuscript received 28 May 2020; accepted manuscript online 12 June 2020)

Tungsten is one of the most promising plasma-facing materials (PFMs) to be used in the nuclear fusion reactor as divertor material in the future. In this work, W^{2+}-ions bombardment is used to simulate the neutron irradiation damage to commercial pure tungsten (W) and rolled tungsten–potassium (W–K). The 7 MeV of 3×10^{15} W^{2+}-ions/cm^2, 3 MeV of 4.5×10^{14} W^{2+}, and 2 MeV of 3×10^{14} W^{2+}-ions/cm^2 are applied at 923 K in sequence to produce a uniform region of 100 nm–400 nm beneath the sample surface with the maximum damage value of 11.5 dpa. Nanoindentation is used to inspect the changes in hardness and elastic modulus after self-ion irradiation. Irradiation hardening occurred in both materials. The irradiation hardening of rolled W–K is affected by two factors: one is the absorption of vacancies and interstitial atoms by potassium bubbles, and the other is the interaction between potassium bubbles and dislocations. Under the condition of 11.5 dpa, the capability of defect absorption can reach a threshold. As a result, dislocations finally dominate the hardening of rolled W–K. Specific features of dislocation loops in W–K are further observed by transmission electron microscopy (TEM) to explain the hardening effect. This work might provide valuable enlightenment for W–K alloy as a promising plasma facing material candidate.

Keywords: plasma facing material, tungsten–potassium alloy, ion-irradiation hardening, nanoindentation

PACS: 52.55.Rk, 61.80.Jh, 28.52.Fa **DOI:** 10.1088/1674-1056/ab9c09

1. Introduction

Tungsten is considered as one of the most promising plasma-facing materials (PFMs) for divertors used in fusion reactor because of its particular properties: high melting point, low sputtering yield, low tritium retention, *etc.*[1,2] Although tungsten has irreplaceable advantages in various properties, its performance changing after irradiation in fusion reactors still needs further studying. Considering that the fusion reactor releases 14-MeV neutrons,[3] which seriously damage PFMs, studies focus on the influence of neutron irradiation on PFMs. So far, the neutron irradiation behaviors of tungsten and various tungsten alloys have been studied. Hu *et al.* investigated the hardening effect of tungsten irradiated by neutrons based on theoretical model prediction and experimental results.[4] Renterghem and Uytdenhouwen investigated the combined irradiation effect of neutrons and electrons on pure tungsten by analyzing post-irradiated dislocation loops and voids.[5] Hwang *et al.* studied the clusters of transmutation elements of tungsten under neutron irradiation and the influence on the properties of PFM.[6] Hasegawa *et al.* revealed the microstructure evolution of W–Re alloy under neutron irradiation.[7] Fujitsuka *et al.* summarized the effects of neutron irradiation on the thermal conductivity of tungsten and tungsten-rhenium alloys.[8]

To some extent it is feasible to simulate the effect of neutron irradiation by using charged ions to study the irradiation damage effect of materials.[9] The reason for this is that the neutron irradiation experiments are very expensive and the time to reach the expected damage value designed in experiment is too long. Moreover, charged particles can not only make the experimental conditions simpler, but also save the time to achieve the necessary displacements per atom (DPA) value, which indicates the degree of irradiation damage. Huang *et al.* found that crystal orientation affects the hardening effect of tungsten irradiated by helium ion.[10] Zhang *et al.* studied the damage behavior of W–Y_2O_3 which had been exposed to 80-eV helium ion irradiation and 1503 K–1553 K thermal shock.[11] Cui *et al.* studied the radiation hardening of tungsten produced by He ion irradiation at 1073 K.[12] El-Atwani discussed loop and void damage during 3-MeV Cu^+ ion irradiating nanocrystalline and coarse grained tungsten at room temperature and 1050 K respectively to investigate the effect of grain size in ion irradiation.[13] Xu *et al.* have systematically studied the clustering and hardening of

*Project supported by the National Natural Science Foundation of China (Grant Nos. 11975160 and 11775149). One of the authors, Kun Zhang, was supported by the Fundamental Research Funds for the Central Universities, China.

†Corresponding author. E-mail: kzhang@scu.edu.cn

‡Corresponding author. E-mail: tangjun@scu.edu.cn

© 2020 Chinese Physical Society and IOP Publishing Ltd

W–Re, W–Re–Os, and W–Re–Ta after being irradiated by ions through using atom probe tomography and nanoindentation measurements.[14,15]

The potassium-doped tungsten (W–K alloy) has proven to possess better mechanical and thermal properties than primitive tungsten.[16,17] In our previous studies, we succeeded in fabricating a series of high-quality W–K alloys by spark plasma sintering (SPS) technology.[18–20] The method of using the heavy ion irradiation is very important for the study of radiation tolerance of the promising PFMs. Tungsten self-ion irradiation can not only produce enough irradiation damage, but also prevent the implanted ions from becoming new impurities to form clusters in the sample. However, up to now, no one has studied the irradiation tolerance of W–K alloy by self-ion irradiation. In this work, rolling technology is used to further process SPS W–K alloy, and W^{2+} self-ion irradiation is carried out on this rolled SPS W–K alloy. Multi-energy ions are chosen to be 7 MeV, 3 MeV, and 2 MeV, in order to obtain an uniform irradiation layer with a high damage level. For comparison, a commercial pure tungsten (W) is irradiated under the same irradiation condition. Nanoindentation and transmission electron microscopy (TEM) are used to investigate the effect of W^{2+} on irradiation hardening of rolled SPS W–K alloy and commercial pure W.

2. Experimental methods

2.1. Sample preparation

The raw material is Al–K–Si (AKS)-doped tungsten powder with purity $>99.9\%$, average particle size of ~ 3.28 μm, from Zigong Cemented Carbide Corporation. In the first step of SPS process, AKS doped tungsten powder was loaded into a graphite mould and preloaded with 40 MPa for 7 min. Then the entire system was ramped up to 1750 °C at a rate of 100 °C/min, kept for 3 min, and hereafter naturally cooled down to room temperature. In the whole sintering process, a pressure of 80 MPa was applied to the graphite mould. The sintering device is shown in Fig. 1. After sintering, the W–K alloy bulk was rolled into a plate (relative density $>99\%$) with a deformation rate of about 80% at 1673 K. After that, we used electrical discharge machining (EDM) to cut the plate into specimens each with a diameter of 15 mm, thickness of 2 mm for the experiments of ion irradiation. Commercially pure W (relative density $>99.9\%$) was selected as reference. The surfaces of all specimens used for irradiation were polished to a mirror surface. Before irradiation, all samples were annealed in vacuum at 1273 K for 2 h in order to remove the stress introduced by the cutting and polishing process.

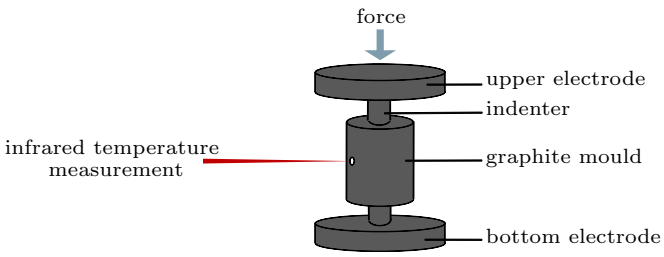


Fig. 1. Schematic diagram of spark plasma sintering (SPS) device.

2.2. W^{2+}-ion irradiation with different ion energies

The irradiation experiment was carried out by using a 3-MV Tandetron accelerator at the Institute of Nuclear Science and Technology, Sichuan University. The samples were irradiated with 7-MeV W^{2+}-ions, 3-MeV W^{2+}-ions, and 2-MeV W^{2+}-ions in sequence. The whole irradiation process was carried out at 923 K within an error of ±10 K. The specimens were mounted on a circular molybdenum holder. The ion beam was perpendicular to the surface of the specimens irradiated uniformly by using beam sweeping system. The stopping range of ions in matter (SRIM) simulation was performed to predict the damage profile in the samples produced by W^{2+}-ions of each energy value. The displacement threshold energy of tungsten was set to be 90 eV and "quick calculation of damage" based on the Kinchin–Pease formalism was the mode for calculation.[21] In order to generate a uniform damage in a range of 100 nm to 400 nm from the surface of irradiated samples, the fluences of tungsten ions with the energy value of 7 MeV, 3 MeV, and 2 MeV were selected to be 3×10^{15} ions/cm^2, 4.5×10^{14} ions/cm^2, and 3×10^{14} ions/cm^2, respectively. Each fluence was converted into a dpa-value (displacements per atom) as shown in Fig. 2.

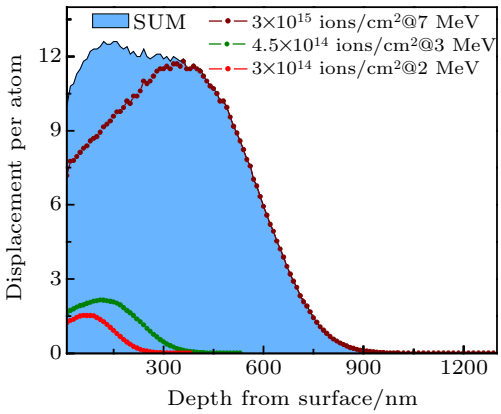


Fig. 2. Damage profiles of self-ion implantation calculated by SRIM mode.

The maximum depth of the irradiation damage was about 1 μm, and a uniform damage value of nearly 11.5 dpa was maintained in a range of 100 nm–400 nm beneath the surface. In a range from 400 nm to 950 nm, the irradiation damage gradually decreased to zero, which was recognized as the damage attenuation region (DAR). Equation (1)[22] shows the method used to extract the dpa from SRIM's output files:

$$\text{dpa} = \frac{F \times \varphi}{\rho} \times 10^8, \tag{1}$$

where F is vacancies/(ions·Å) from the vacancy.txt in the output files generated by SRIM mode, ϕ is the ion-beam fluence (ions/cm^2), ρ is the atom density (atoms/cm^3) of irradiated sample.

2.3. Nanoindentation and TEM

Nanoindentation was characterized by a nanoindenter facility (EMS-60, Agilent Technologies). Continuous stiffness measurements (CSM) were used to measure the hardness as a function of indentation depth without needing to runmultiple load–unload cycles.[23] The hardness was measured by imposing a signal (2 nm at 45 Hz) on the load-displacement curve. In order to reduce the measurement error, each sample was indented 15 times. The maximum indentation depth was 2 μm, which could cover the entire irradiation region. The Oliver–Pharr method[24] was used to calculate hardness. Transmission electron microscopy (TEM, FEI Tecnai G2 F20) was used to characterize the defect in the W^{2+}-ion damaged region. The TEM lamellae each with a thickness of ≈ 100 nm were prepared by the focused ion beam (FIB, FEI Helio600i). As the length of the lamellae is over 3 μm, both the irradiated range (∼ 1 μm based on SRIM) and unirradiated range could be covered. Scanning electron microscope (SEM) (S4800, Hitachi, Japan) with an acceleration voltage range of 15 kV–20 kV was employed to characterize the surface morphology. Traditional x-ray diffraction (XRD) (DX2700, Haoyuan, China) scanning was also utilized in this work in steps of 0.01°.

3. Results

Representative load versus displacement (indenter depth) curves for irradiated and unirradiated pure W and rolled W–K are shown in Fig. 3. It is obvious that after irradiation the value of load on sample becomes higher for both pure W and rolled W.

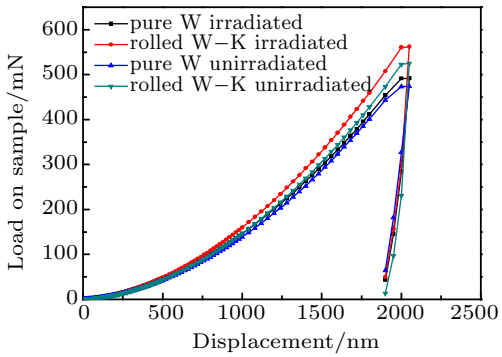


Fig. 3. Nanoindentation measured load displacement curves for pure tungsten and rolled W–K before and after irradiation.

Figures 4(a) and 4(b) show the plots of hardness versus displacement for the same samples. The hardness is obtained by using the load displacement curve and Oliver–Pharr method.[24] In a range of 0 nm–100 nm, the hardness value has great deviation due to the surface roughness. In the range of 100 nm–400 nm where the SRIM simulation result shows a maximum and uniform irradiation damage, the hardness of irradiated rolled W–K and pure W increases. In the DAR, the hardness of the irradiated sample gradually approaches to that of the non-irradiated sample, and the trend of pure W is more obvious. At 1200 nm below the surface, the hardness value of the irradiated sample still increases.

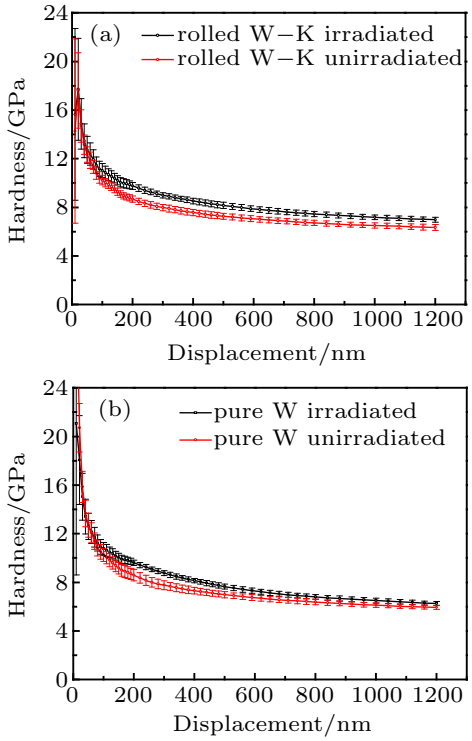


Fig. 4. Hardness *versus* displacement for (a) rolled W–K and (b) pure W, showing an increase in hardness after self-ion irradiation.

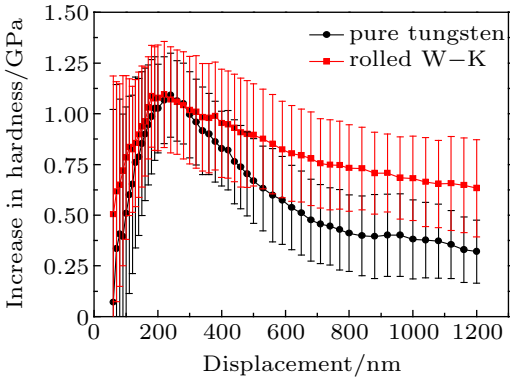


Fig. 5. Hardness decreasing with displacement increasing for rolled W–K and pure W after self-ion implanted.

Figure 5 shows an increase in hardness as a function of displacement for pure W and rolled W–K before and after being implanted by ions in order to show the change of hardness after irradiation more intuitively. The initial hardness of unirradiated rolled W–K and pure W are 8.95 ± 0.25 GPa and 8.58 ± 0.47 GPa, respectively. At a damage value of 11.5 dpa produced by multi-energy W^{2+}-ions's irradiation, the hardness of rolled W–K increases to 9.98 ± 0.38 GPa. The pure W has a significant increase in hardness to 9.61 ± 0.22 GPa after self-ion irradiation. There remains an increase in hardness of

approximately 0.32±0.17 GPa in pure W and 0.64±0.24 GPa in rolled W–K at a depth of 1.2 μm which is considered as an uninfluenced range. It is proposed that a surface layer with enhanced hardness still exerts a remarkable influence on the hardness achieved by this method, even when the indent depth reaches the range, showing that it is relatively soft.[23]

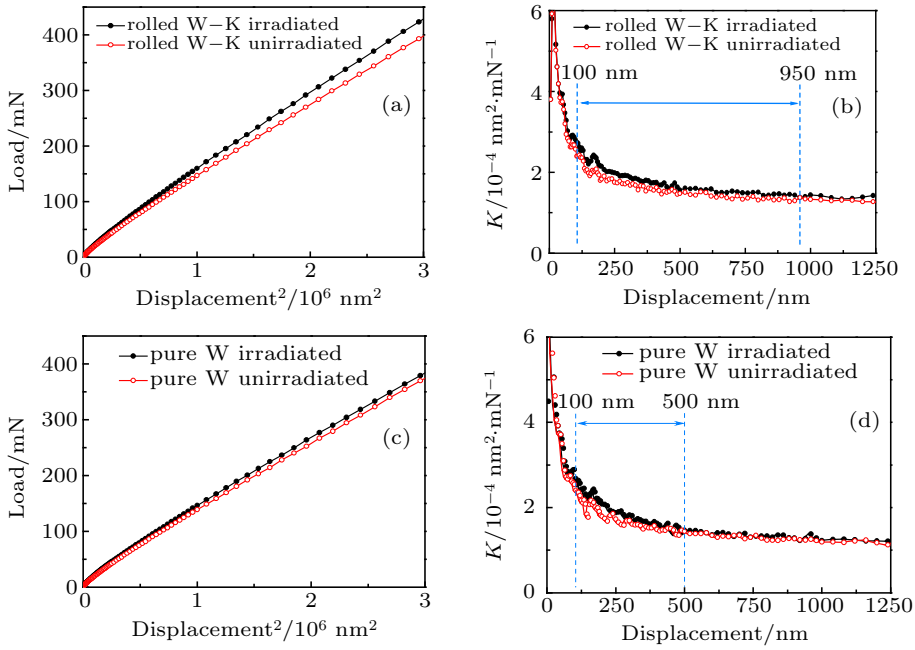


Fig. 6. Load–diaplacement^2 (P–δ^2) curves for (a) pure W and (c) rolled W–K, unirradiated and irradiated. Gradient (K) of P–δ^2 lines (b) in panel (a) and (d) in panel (c) *versus* displacement.

Apparent hardening effect is observed in the both irradiated samples. However, by comparison, the actual irradiation damage depth of the material may be different from that of SRIM simulation. It is difficult to determine the depth of damage caused by ion irradiation based on the measured hardness value. So far, there have been many studies using nanoindentation to evaluate the properties of thin coatings. However, such research cases are all on condition that the coating and the substrate have significant difference in performance, such as a hard coating on a soft substrate or a soft coating on a hard substrate. It is found in the Bull's study that in general, when the measured thickness does not exceed 10% of the coating thickness, the measurement results will not be significantly influenced by the substrate.[25] The irradiation influence layer can be considered as coating on the unirradiated region. In this study, the thickness of the irradiated layer is about 1000 nm. Therefore, this approach is unfeasible since the data from the first 100-nm depth are badly influenced by initial pop-ins, surface roughness and tip shape effects. Hainsworth *et al.*[26] revealed that the plot of load *versus* displacement squared (P–δ^2) for a homogeneous material should be a straight line. McGurk and Page have shown that in the case of a hard coating on substrate the properties of the coating can be deconvoluted from the influence of the substrate by using an analysis of such P–δ^2 plots.[27] They plotted the gradient (K) of the P–δ^2 curve as a function of indentation displacement and proved that by this method, the coating area and the substrate area can be determined by comparing the areas with different gradients on the plot. Here we use the method described in Refs. [26,27] to analyze the actual depth of irradiation damage layer. Figure 6(a) shows a plot of P–δ^2 for the indentations for irradiated and unirradiated rolled W–K. The gradient of the plot of P–δ^2 in Fig. 6(a) is calculated by the least square method of linear regression, and the results are plotted as the gradient *versus* indentation displacement in Fig. 6(b). The P–δ^2 curves and the gradient-displacement curves of irradiated and unirradiated pure W calculated by the same method are shown in Figs. 6(c) and 6(d), respectively. It can be seen from Figs. 6(a) and 6(c) that the curves after irradiation deviate significantly from those before irradiation, which indicates that the properties of ion irradiated layer are changed no matter whether it is pure W or rolled W–K. It can be noted that the data below 50 nm–60 nm is not credible due to the influence of the surface tip shape effect and initial pop-in in pure tungsten and rolled W–K. There is a significant difference that the gradient of the plot of P–δ^2 for the implanted rolled W–K is obviously higher than that for the unirradiated rolled W–K in the range of 100 nm–500 nm. In the range of 500 nm–950 nm, the curve of the irradiated rolled W–K shifts towards the curve of the unirradiated rolled W–K slowly. Above 950 nm, the difference between the two lines of the irradiated and unirradiated rolled W–K is not apparent. There is a good correlation between the thickness of the layer affected by ion irradiation in rolled W–K obtained by using an analysis of K-displacement plots and the result calculated by SRIM. In Fig. 6(d), there is a clear difference between 100 nm and 300 nm, which can be observed with the implanted layer, showing a significantly higher gradient in pure W, which is exactly corresponding to an increase

in hardness of the layer over the unimplanted region. In the range of 300 nm–500 nm, the curve of the irradiated pure W rapidly shifts towards the unirradiated pure W's line. And no significant difference is observed between the two lines above 500 nm. From the curve analysis in Fig. 6(d), the depth of the irradiation influence layer of pure W is smaller than that of SRIM simulation.

The TEM is used to observe the 11.5-dpa damage region and the DAR of pure tungsten and rolled W–K alloy, and the results are shown in Figs. 7. The red arrow in Fig. 7(b) points to the sample surface. Figures 7(b) and 7(d) display massive dislocation loops in both pure tungsten and rolled W–K alloy after being bombarded by W^{2+} ions. However, areas with much lower density of irradiation-induced defects can be found in the DARs of two materials as shown in Figs. 7(c) and 7(e). The density of dislocation loops in the DAR of rolled W–K alloy seems to be higher than that in the pure tungsten, which may be caused by the pinning effect of the potassium bubbles. However, some differences of this region can be argued. In the selected region of the DAR of rolled W–K alloy as shown in Fig. 7(c), the distribution of dislocation loops is not uniform. On the edge of the selected region of the DAR of pure tungsten some dislocation loops are apparent. The inhomogeneous distribution of dislocation loops may be due to the recombination and rearrangement of irradiation defects. The different mobilities of irradiation defects in rolled W–K alloy and pure tungsten will lead to different dislocation loop densities and size distributions in the two materials. This may be the reason why the hardness of DAR changes more significantly in rolled W–K after being irradiated by ions as shown in Fig. 5.

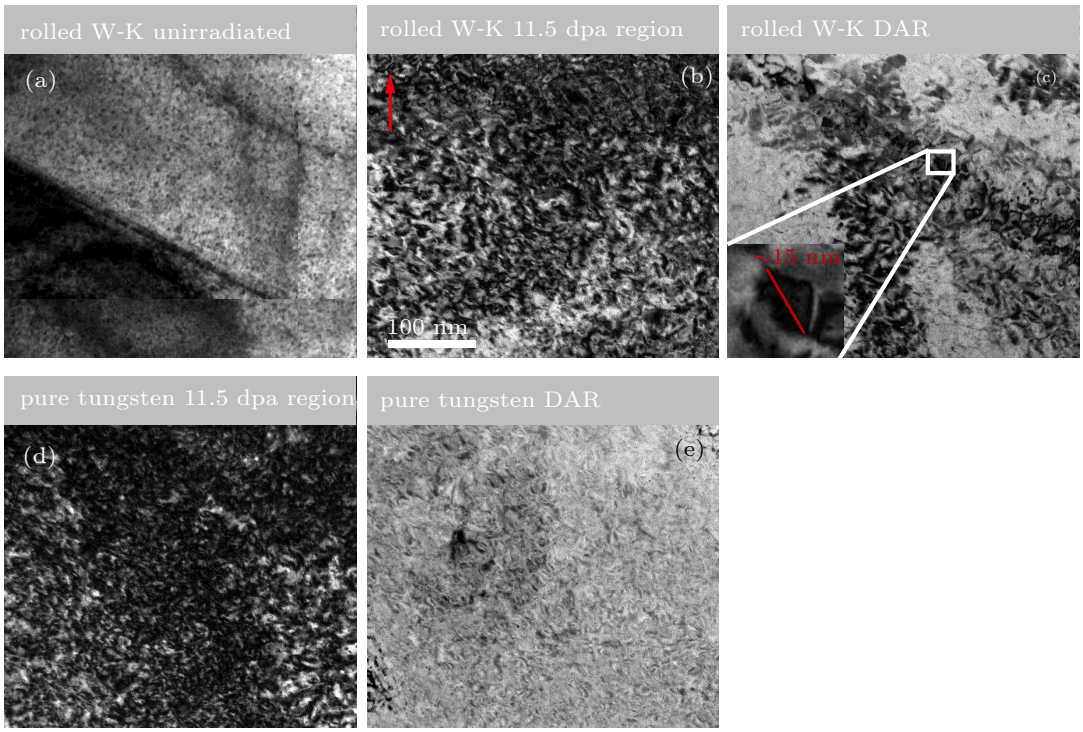


Fig. 7. TEM images of dislocation loops in pure W and rolled W–K irradiated to 11.5-dpa damage (TEM bright field images): (a) unirradiated W–K; (b) 11.5-dpa region of rolled W–K; (c) DAR of rolled W–K; (d) 11.5-dpa region of pure W; (e) DAR of pure W. All images have the same scale bar of 100 nm. Red arrow points to top surface of sample, and white box highlighting area enlarged shows dislocation loops of around 15 nm in size.

The SEM surface morphologies of the samples are shown in Fig. 8. Self-ion irradiation causes sputtering damage to the surface of pure tungsten and rolled W–K alloy sample. It can be seen from Figs. 8(a) and 8(b) that the surface of pure tungsten sample has a large area of pits due to the sputtering effect of ion bombardment. For the rolled W–K, irradiation-induced pits are also observed as shown in Figs. 8(c) and 8(d). However, the depths of these pits seem much smaller than those in the case of pure tungsten. We further notice that the morphology with the appearance looking like the grain boundaries and sub grain boundaries occurs on the surface of the rolled W–K alloy, which may be due to the lower sputtering threshold in these regions in rolled W–K alloy. Detailed mechanism for the formation of sputtering pits needs further investigating.

Figure 9(a) shows the elasticity modulus results of pure tungsten and rolled W–K samples before and after being irradiated by ions. After being irradiated by 11.5-dpa tungsten self-ion irradiation, the pure tungsten has the modulus significantly increasing from 431.09 ± 16.13 GPa to 481.33 ± 11.27 GPa. In the case of rolled W–K alloy, the variation is negligible (from 449.87 ± 13.97 GPa to 442.91 ± 28.61 GPa). It may be attributed to the absorption effect of potassium bubbles on irradiation-induced defects, which will be discussed in the following section. In Fig. 9(b), the XRD patterns indicate that neither grain size nor distinct γ-phase in pure tungsten or rolled W–K alloy has obvious change.

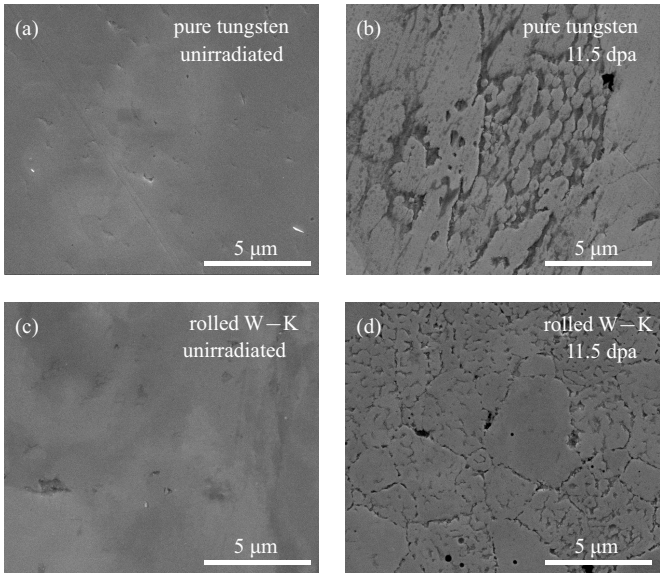


Fig. 8. (a) Surface morphology of pure W unirradiated. (b) Surface morphology of pure W irradiated. (c) Surface morphology of rolled W–K unirradiated. (d) Surface morphology of rolled W–K irradiated.

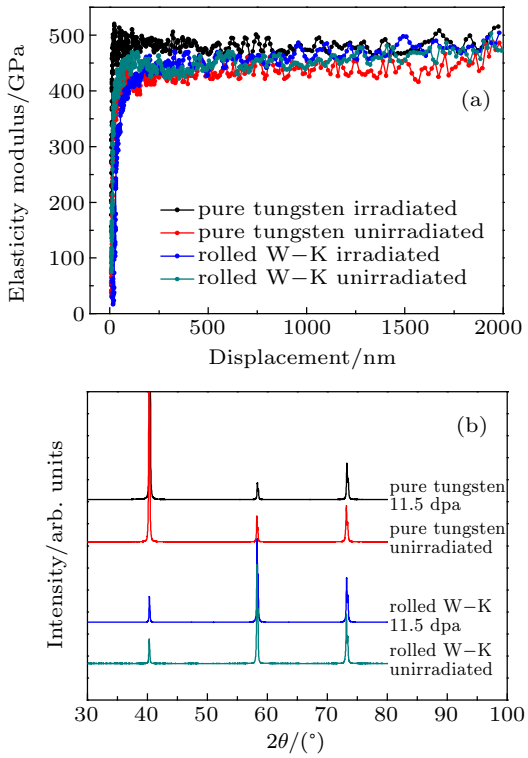


Fig. 9. (a) Elasticity moduli of pure tungsten and rolled W–K alloy samples. (b) XRD spectra of tungsten self-ions irradiated samples with black line representing the pure tungsten after being irradiated, red line the pure tungsten before being irradiated, blue line the W–K alloy after being irradiated , and green line the W–K alloy before being irradiated.

4. Discussion

Through comparison, it is found that although the irradiation depth predicted with SRIM is in good agreement with the result measured by nanoindentation and the result measured from TEM images, there are still some results to be argued. Although the maximum value of hardness increase of the rolled W–K alloy is almost the same as that of the pure tungsten, the irradiation hardening effect of the rolled W–K alloy is more obvious in the deeper region as shown in Fig. 5. These may be explained in terms of recombination and rearrangement of defects.[28] According to previous research, the two main driving forces that affect the mobility of defects in material microstructure are produce from stress field and temperature, respectively. Although the migration of defects in tungsten is very slow at room temperature,[29] the mobility of defects increases when the temperature is higher than 720 K.[30] Considering the fact that the temperature is 923 K during the irradiation, it is possible that the dislocation loop produced by the irradiation of W^{2+}-ions has good mobility. Sakamoto *et al.* found that at 473 K and above, the dislocation loops produced by hydrogen ion irradiation will escape to the surface of tungsten.[31] In our previous work, Huang *et al*. found that the potassium bubbles dispersed in tungsten can store and lock dislocations.[32] According to the analysis of nanoindentation test results in Fig. 6 and the observed microstructure characteristics of the samples in Fig. 7, we speculate that at 923 K, the irradiation defects in pure tungsten have higher mobility due to the pinning effect of potassium bubbles on the irradiation defects in the W–K alloy. After the recombination and rearrangement of irradiation defects, the DAR of the rolled W–K alloy may have a higher irradiation defect density, which may affect the trend of hardness change of the rolled W–K alloy and lead the rolled W–K alloy in DAR to more harden than the pure tungsten. According to our previous research, the irradiation hardening value of pure tungsten is much higher than that of rolled W–K alloy when the damage value is relatively low (3 dpa, 5 dpa, and 8 dpa at 923 K).[33] When the irradiation damage value reaches 11.5 dpa, the peak hardness of pure tungsten increases by 12.0%, while that of the rolled W–K alloy increases by 11.5%. It is speculated that the improvement of the irradiation hardening resistance of the rolled W–K alloy is due to the combination of the absorption of the vacancy and interstitial atoms by the potassium bubbles, together with the distribution of the irradiation-induced dislocation loops. With the accumulation of irradiation damage, the potassium bubbles can only absorb a limited quantity of irradiation defects. Therefore, as the irradiation dislocation loops continue to produce, the rolled W–K alloy may gradually lose the advantage of irradiation hardening resistance. The distribution and evolution of dislocation loops induced by irradiation in rolled W–K alloys need further studying.

From Fig. 8, we can see the effects of tungsten self-ion irradiation on the surface morphology of pure tungsten and rolled W–K alloy. Potassium doping may improve the sputtering resistance of tungsten, but the improvement also varies with the grain orientation. From Fig. 8(d), the sputtering damages in the grains with various orientations turned out to be greatly different and the doping of potassium seems to have an adverse effect on the ability of the grain boundaries to sup-

press sputtering. Nevertheless, we believe that the rolled W–K alloys still have room to improve the anti-sputtering ability if the potassium bubbles can be further refined.

The elasticity modulus of pure tungsten and rolled W–K alloy are shown in Fig. 9(a). The modulus of rolled W–K alloy does not dramatically vary after being irradiated, but that of pure tungsten increases by approximately 11.7%. According to the XRD patterns shown in Fig. 9(b), we can ensure that there is no phase transformation nor new chemical composition formation in pure tungsten and rolled W–K alloy during the irradiation. As a bcc structure, the factors affecting the modulus during irradiation should be the vacancies and interstitial atoms produced by self-ion bombardment.[34] The interstitial atoms can increase the modulus, while the vacancies can reduce the modulus. The contribution of interstitial atoms to the modulus is much greater than that of vacancies. The increase of the modulus of pure tungsten after being irradiated is probably caused by a large number of interstitial atoms. However, the modulus of the rolled W–K alloy does not change much. The possible reason is that potassium bubbles absorb most of the irradiation defects such as vacancies and interstitial atoms.

5. Conclusions

In this work, we prepare rolled W–K samples by SPS and rolling methods. Multi-energy W^{2+}-ions are chosen to implant the samples of rolled W–K and commercial pure W. In this way, we achieve nearly uniform irradiation damage ($\sim$ 11.5 dpa) in a depth range of 100 nm–400 nm beneath the sample surface. Through the observation of the surface morphology of the samples, the rolled W–K alloy seems to have better anti-sputtering ability than pure tungsten, which is beneficial to the stability of the plasma in fusion reactors. In the 11.5-dpa damage region, the increments in hardness of pure W and rolled W–K are almost identical, while the hardness of rolled W–K is distinctly higher in the region of DAR, in which more dislocations are found through the TEM observation. The interaction between K-bubbles and dislocations results in a relatively low mobility of dislocation loop in rolled W–K compared with the scenario in the pure tungsten. Therefore, W–K has more dislocation loops and obvious hardening in the DAR region. In the case of pure tungsten, there are less dislocation loops and less hardening because the dislocation loops tend to migrate to the surface at 923 K. When the irradiation damage is low, the dislocation loops produced by irradiation are quite few. Thus, the absorption of vacancies and interstitial atoms by potassium bubbles significantly reduces the irradiation hardening. With the accumulation of irradiation damage, a threshold ($\sim$ 11.5 dpa) is reached, and the positive effect of defect absorption will weaken gradually. On the other hand, the hardening effect of dislocation loops becomes dominant. Ultimately, the irradiation hardening tolerance of W–K is attenuated. We believe, increasing the threshold might be the key to improving the irradiation hardening resistance of W–K.

References

[1] Hu X, Koyanagi T, Fukuda M, Katoh Y, Snead L L and Wirth B D 2016 *J. Nucl. Mater.* **470** 278
[2] Yang X L, Qiu W B, Chen L Q and Tang J 2019 *Tungsten* **1** 141
[3] You Y W, Kong X S, Wu X B, Liu C S and Chen J L 2017 *Nucl. Fusion* **57** 016006
[4] Hu X X, Koyanagi T, Fukuda M, Kumar N A P L, Snead L L, Wirth B D and Katoh Y 2016 *J. Nucl. Mater.* **480** 235
[5] Renterghem W V and Uytdenhouwen I 2016 *J. Nucl. Mater.* **477** 77
[6] Hwang T, Hasegawa A, Tomura K, Ebisawa N, Toyama T, Nagai Y, Fukuda M, Miyazawa T, Tanaka T, Nogami S 2018 *J. Nucl. Mater.* **507** 78
[7] Hasegawa A, Fukuda M, Yabuuchi K and Nogami S 2016 *J. Nucl. Mater.* **471** 175
[8] Fujitsuka M, Tsuchiya B, Mutoh I, Tanabe T and Shikama T 2000 *J. Nucl. Mater.* **283–287** 1148
[9] Ogorodnikova O V and Gann V 2015 *J. Nucl. Mater.* **460** 60
[10] Huang S L, Ran G, Lei P H, Chen N j, Wu S H, Li N and Shen Q 2017 *Nucl. Instrum. Method B* **406** 585
[11] Zhang Y X, Tan X Y, Luo L M, Xu Y, Zan X, Xu Q, Tokunaga K, Zhu X Y and Wu Y C 2019 *Fusion Eng. Des.* **140** 102
[12] Cui M H, Shen T L, Zhu H P, Wang J, Cao X Z, Zhang P, Pang L L, Yao C F, Wei K F, Zhu Y B, Li B S, Sun J R, Gao N, Gao X, Zhang H P, Sheng Y B, Chang H L, He W H and Wang Z G 2017 *Fusion Eng. Des.* **121** 313
[13] El-Atwani O, Esquivel E, Efe M, Aydogan E, Wang Y Q, Martinez E and Maloy S A 2018 *Acta Mater.* **149** 206
[14] Xu A, Beck C, Armstrong D E J, Rajan K, Smith G D W, bagot P A J and Roberts S G 2015 *Acta Mater.* **87** 121
[15] Xu A, Armstrong D E J, Beck C, Moody P M, Smith G D W, Bagot P A J and Roberts S G 2017 *Acta Mater.* **124** 71
[16] Huang B, Chen L Q, Qiu W B, Yang X L, Shi K, Lian Y Y, Liu X and Tang J 2019 *J. Nucl. Mater.* **520** 6
[17] Nogami S, Watanabe S, Reiser J, Rieth M, Sickinger S and Hasegawa A 2019 *Fusion Eng. Des.* **140** 48
[18] Huang B, Xiao Y, He B, Yang J J, Liao J L, Yang Y Y, Liu N, Lian Y Y, Liu X and Tang J 2015 *Int. J. Refract. Met. Hard Mater.* **51** 19
[19] He B, Huang B, Xiao Y, Lian Y Y, Liu X and Tang J 2016 *J. Alloys Compd.* **686** 298
[20] Xiao Y, Huang B, He B, Shi K, Lian Y Y, Liu X and Tang J 2016 *J. Alloys Compd.* **678** 533
[21] Ogorodnikova O V, Tyburska B, Alimov V K and Ertl K 2011 *J. Nucl. Mater.* **415** S661
[22] Egeland G W, Valdez J A, Amloy S A, McClellan K J, Sickafus K E and Bond G M 2013 *J. Nucl. Mater.* **435** 77
[23] Wang K, Qi Q, Cheng G J and Shi L Q 2014 *Chin. Phys. Lett.* **31** 072801
[24] Li X D and Bhushan B 2002 *Mater. Charact.* **48** 11
[25] Bull S J 2005 *J. Phys. D: Appl. Phys.* **38** R393
[26] Hainsworth S V, Chandler H W and Page T F 1996 *J. Mater. Res.* **11** 1987
[27] McGurk M R and Page T F 1999 *J. Mater. Res.* **14** 2283
[28] Ciupiński Ł, Ogorodnikova O V, Płociński T, Andrzejczuk M, Rasiński M, Mayer M and Kurzydłowski K J 2013 *Nucl. Instrum. Method B* **317** 159
[29] Gilbert M R, Dudarev S L, Derlet P M and Pettifor D G 2008 *J. Phys.: Condens. Matter* **20** 345214
[30] Keys L K, Smith J P and Moteff J 1968 *Phys. Rev.* **176** 851
[31] Sakamoto R, Muroga T and Yoshida N 1995 *J. Nucl. Mater.* **220–222** 819
[32] Huang B, Tang J, Chen L Q, Yang X L, Lian Y Y, Chen L, Liu X, Cui X D, Gu L and Liu C T 2019 *J. Alloys Compd.* **782** 149
[33] Yang X L, Chen L Q, Qiu W B, Song Y Y P, Tang Y, Cui X D, Liu C S, Jiang Y, Zhang T and Tang J 2020 *Chin. Phys. B* **29** 046102
[34] Li W N, Xue J M, Wang J X and Duan H L 2014 *Chin. Phys. B* **23** 036101